PAPER

Design of Multiple-Receiving WPT System Using Ferrite-Embedded LTCC

Young-Hyun KIM[†], **Dae-Kil PARK**[†], ***and*** **Kyung-Heon KOO**[†a)], ***Members***

SUMMARY Wireless power transfer (WPT) can be classified into magnetic induction, magnetic resonance, and RF radiation types, of which the magnetic resonance WPT system is especially attracting attention due to its high potential for development. The magnetic resonance system using a specific resonance frequency is applicable to small mobile devices and in-body wireless charging modules because it enables the implementation of single-input multiple-output (SIMO), where the transmitter transmits power to multiple receivers, and the miniaturization of receiving coil. The most important consideration of the magnetic resonance WPT is the optimization of the power transfer distance and efficiency, which requires a precise design and the analysis of the transmission coil. Ferrite-embedded LTCC inductors are more advantageous for WPT applications than coil inductors because of their low cost, batch manufacturing and durability. A coil with the substate size of $10.0 \times 12.0 \times 0.7\,\mathrm{mm}^3$ was manufactured using the ferrite-embedded LTCC technology to miniaturize the receiver coil. The sum of power transferred from transmitter sized of $80 \times 60\,\mathrm{mm}^2$ to two receivers is approximately 32%, which indicates a high potential for use in small terminals or in-body modules.

key words: *WPT, magnetic resonance, LTCC, ferrite*

1. Introduction

A system with midium power transfer and optimal efficiency for multiple outputs has been proposed as a result of continuous research on the magnetic resonance wireless power transfer (WPT). In addition, the attempts have been made to apply a wireless charging system to mobile devices such as smartphone and tablet, which are equipped with single-input multiple-output (SIMO) systems through the development of the transmitter and receiver with high compatibility [1]–[3]. The minimization of the receiving coil enables the development of smaller mobile devices and ultimately application to more convenient and various environments such as wireless charge used in implantable medical devices [4]–[6]. Since the use of batteries in implantable device has some risks, the wireless charge is a feasible alternative. Compared with the receiving part, there are many cases where the transmitting part is not limited in size and shape. To miniaturize the receiving part, the FR-4 printed circuit board (PCB) [7]–[9] or complementary metal-oxide semiconductor (CMOS) [10], [11] process has been used.

This study has adopted and modified the low-temperature co-fired ceramic (LTCC) technique [12], where a NiZn ferrite sheet is embedded between ceramic sheets to increase inductance value was used for the minimization. The LTCC receivers are designed so that the amount of power transferred is higher than other types of receivers, and minimize the commercialized product. These LTCC products are made by laminating ceramic sheets and characterized by more rigid and cheap materials. The inductance realized by this technique has effect of decreasing the parasitic elements, meaning that the application of the embedded passive technique is possible for the minimization and integration. Two types of receivers were mathematically modeled by constructing the SIMO-based WPT system, and the efficiency was analyzed for each case.

2. Inductor Realization on the Ferrite-Embedded LTCC

An inductance that can secure a sufficient electromotive force to compensate for the characteristics of the LTCC for wireless power transfer is required. Ferrite sheet with large relative permeability (i.e. 40) was built in to miniaturize the inductor. A higher permeability is achieved when the sintering is performed at a temperature closer to the melting point. NiZn ferrite enables sintering at high temperatures, but its weakness is the high resistance of the internal conductor, which is solved by using Ag as a conductor to maintain a high Q value. An inductor fabricated using only a ferrite layer has poor surface roughness and low strength, which makes packaging difficult. To overcome these disadvantages, we fabricated a ceramic-ferrite-ceramic sandwich structure to improve the matching of each sheet and distribute the structural stress.

The manufacturing process of the LTCC inductor with built-in ferrite is as follows: LTCC powder and NiZn ferrite to form an inductor were mixed with a binder solution and a solvent to prepare the slurry for tape casting. After this slurry had been pulverized twice, tape casting was performed with a blade gap of 420 μm, so that the cast and dried tape was 100–110 μm thick, which resulted in a ferrite-LTCC composite green sheet. The vias for the internal electrical connection across the circuit layers were formed by mechanical punching following the circuit layout. After the vias were filled, a coil with a gap of 400 μm was designed and screen-printed on each layer. The entire layers including the vias and coils were laminated; then, the laminated components were sintered together. The castellation for the electrode formation on the sintered ferrite-LTCC composite structure was performed,

Manuscript received January 8, 2019.
Manuscript revised July 24, 2019.
Manuscript publicized September 20, 2019.

[†]The authors are with Department of Electronics Engineering, Incheon National University, Incheon, Korea.
a) E-mail: khkoo@inu.ac.kr

DOI: 10.1587/transcom.2019EBP3008

Table 1 Key determinants of the LTCC inductor.

Device property	Key determinants
Inductance [H]	Line width and space Inner radius Number of turns Metal thickness
Quality factor	Metal thickness Line width
Tolerance [%]	Metal line width Thickness variation
Self-resonant frequency	Inductor area Substrate dielectric constant
Series resistance R_S [Ω]	Metal thickness Metal line width Total length
Parallel capacitance C_P [F]	Line space Inductor area
Resistance to ground R_G [Ω]	Substrate conductivity (loss tangent)
Capacitance to ground R_G [Ω]	Inductor area Separation from ground Substrate dielectric constant

Table 2 Ferrite-embedded LTCC receiving coil parameters.

Ferrite Sheet	
Dielectric constant	50
Permeability	40
Thickness [μm]	100
Loss tangent	0.004
Conductor(Ag)	
Thickness [μm]	12
Resistivity [Ωm]	$2.4 * 10^{-8}$
Line width / space (min.) [μm]	200
Via diameter [μm]	300
Ceramic Sheet	
Dielectric constant	7.5
Thickness [μm]	100
Loss tangent	0.003

and AgPd pastes were printed. The ceramics were produced at the peak temperature of 780°C.

The LTCC, including the fabricated ferrite, is designed to minimize the resistance and has a spiral conductor loop structure with the inductance of at least 2 μH. In designing, the trade-off between inductance and resistance should be considered, and the conductors should be placed as close as possible to increase the mutual inductance, and the line length need to be minimized to decrease the resistance. The inductor shape is classified into loop, meander, spiral and others. In fabrication, the Q-factor, maximum allowable current due to the conductor resistance, and self-resonant frequency (SRF) of the inductor need to be carefully monitored.

Table 1 shows the important performance metrics of ferrite-embedded LTCC inductors. Table 2 shows the physical properties in the proposed ferrite-embedded LTCC structure.

Figure 1 shows the ferrite-embedded LTCC designed with a 3D simulator. Figures 2 and 3 are the drawings of each layer. Among seven layers, ferrite occupies the 2nd–6th layers, and ceramic occupies the 1st and 7th layers, which

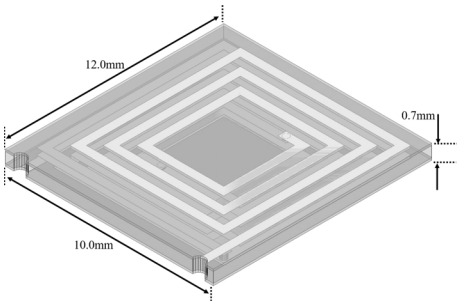

Fig. 1 Designed ferrite-embedded LTCC ($10.0 \times 12.0 \times 0.7\,\mathrm{mm}^3$).

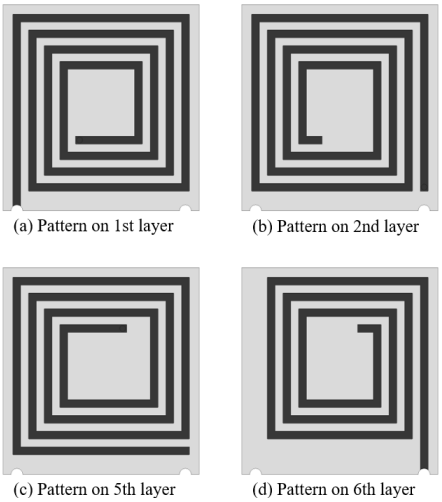

Fig. 2 Conductor pattern on each layer of the ferrite-embedded LTCC.

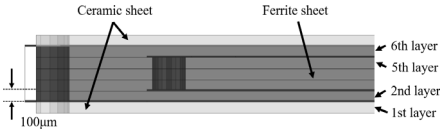

Fig. 3 Cross section of the ferrite-embedded LTCC. Each layer has 100 μm thickness.

form a sandwich structure. The conductor lines of the top and bottom layers were designed to locate outside the ferrite to have a rectangular spiral structure and identical current direction at each layer.

Figure 4 shows the simulation performed at a structure and various frequencies to compare the characteristics of the existing LTCC, which consists of ceramic only and the proposed LTCC with built-in ferrite using FEM based EM simulation. Q-factor can be obtaind as ωL/R, where ω is angular frequency, L is inductance, and R is resistance. According to Fig. 4, Q-factor increases with increasing frequency. The inductance and Q-factor are 1.8 μH and 18, respectively, in the existing LTCC which are lower than the valued in the proposed LTCC (2.4 μH and 30). At 6.78 MHz, the inductance and Q-factor of the proposed LTCC are 2.43 μH and 25, respectively, which are much larger than the values of the conventional LTCC (i.e. 1.75 μH and 17) for the same size as shown in Fig. 4. Conventional LTCC is difficult to

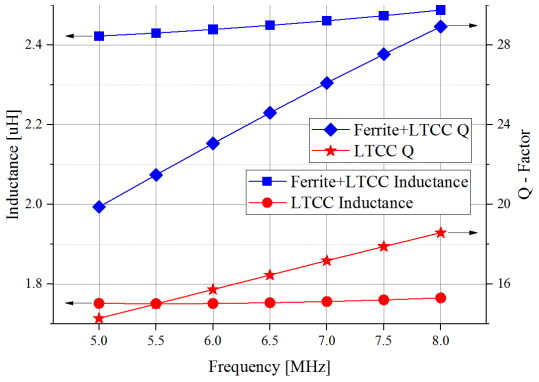

Fig. 4 Comparisons of inductance and Q-factor for the proposed ferrite-embedded LTCC and the conventional LTCC by using FEM based EM simulation.

use for small size receiver. Proposed receiver has 40% larger inductance and 47% higher Q-factor.

3. System Model Analysis

Figure 5 shows the proposed magnetic resonant wireless power transfer system with the transmitter and ferrite-embedded LTCC for the receivers. The loop coil for power feeding is arranged at interval of 1.0 mm from the resonance coil. Resonant coil and the receivers maintain a vertical 5.0 mm interval. Figure 6 shows the equivalent circuit of the proposed system. The current, voltage, and magnetic coupling of each coil are expressed by Kirchhoff equation in Eq. (1), and each impedance is expressed in Eq. (2) [13]–[15].

$$\begin{bmatrix} V_S \\ 0 \\ 0 \\ 0 \end{bmatrix} = \begin{bmatrix} Z_1 & j\omega M_{21} & 0 & 0 \\ j\omega M_{12} & Z_2 & j\omega M_{32} & j\omega M_{42} \\ 0 & j\omega M_{32} & Z_3 & 0 \\ 0 & j\omega M_{32} & 0 & Z_4 \end{bmatrix} \begin{bmatrix} I_1 \\ I_2 \\ I_3 \\ I_4 \end{bmatrix} \quad (1)$$

$$Z_1 = Z_S + R_1 + j\omega L_1 \quad (2)$$

$$Z_2 = R_2 + j(\omega L_2 - 1/\omega C_2) \quad (3)$$

$$Z_3 = Z_L + R_3 + j(\omega L_3 - 1/\omega C_3) \quad (4)$$

$$Z_4 = Z_L + R_4 + j(\omega L_4 - 1/\omega C_4) \quad (5)$$

In Eq. (1), $M_{nm} = M_{mn}$. Currents I_3 and I_4 flow through ferrite-embedded LTCC for the receivers, and the voltages V_{L3} and V_{L4} can be obtained.

$$V_{L3} = I_3 Z_L \quad (6)$$

$$V_{L4} = I_4 Z_L \quad (7)$$

If receivers with the same electrical characteristics are placed at the constant interval with symmetric position from the resonant coil, the impedance of each ferrite-embedded LTCC is equal to Z_3=Z_4 and M_{23}=M_{24}. the currents I_3 and I_4 are summarized as shown in Eq. (8).

$$I_3 = I_4 = \frac{\omega^2 M_{12} M_{23} V_S}{2\omega^2 M_{23}^2 Z_1 + 2\omega^2 M_{12}^2 Z_3 + Z_1 Z_2 Z_3} \quad (8)$$

In the equivalent circuit of Fig. 6, the 3-port network excludes

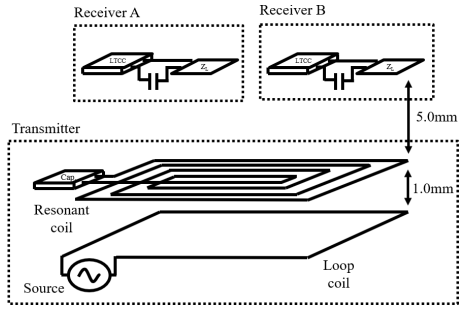

Fig. 5 Schematic of the WPT system with ferrite-embedded LTCC receivers.

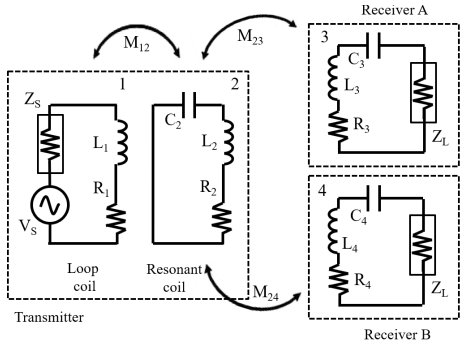

Fig. 6 Equivalent circuit of the WPT system with LTCC receivers

Table 3 Size and Inductance of the loop coil and resonant coil. l1 or l2 is the side length of the resonant and loop coil. w is diameter of the wire. s is space between wires of the resonant coil. N is the nunber of turns for the resonant coil.

	l1 [mm]	l2 [mm]	w [mm]	s [mm]	N [turns]	Inductance [μH]
Loop coil	80.0	60.0	0.6	-	-	0.264
Resonant coil	80.0	60.0	0.6	2.0	10	5.41

the transmission resonance coil, and the efficiency can be calculated from S_{21} and S_{31} of the system. S_{21} and S_{31} are expressed by Eq. (9).

$$S_{21} = S_{31} = 2\frac{V_{L3}}{V_S}\sqrt{\frac{Z_S}{Z_L}} = 2\frac{V_{L4}}{V_S}\sqrt{\frac{Z_S}{Z_L}} = \frac{2\omega^2 M_{12} M_{23} Z_L \sqrt{\frac{Z_S}{Z_L}}}{2\omega^2 M_{23}^2 Z_1 + 2\omega^2 M_{12}^2 Z_3 + Z_1 Z_2 Z_3} \quad (9)$$

The change in transmission distance affects the mutual inductance and consequently the overall system efficiency and input/output impedances.

Table 3 shows the size and inductance of the proposed transmission loop coil and resonant coil.

Figure 7 shows the change in mutual inductance according to the position change between the transmitting resonant coil and the ferrite-embedded LTCC. The vertical distance between the transmitting resonant coil and the ferrite-embedded LTCC is 5.0 mm. The change in mutual inductance between them within the transmission area according

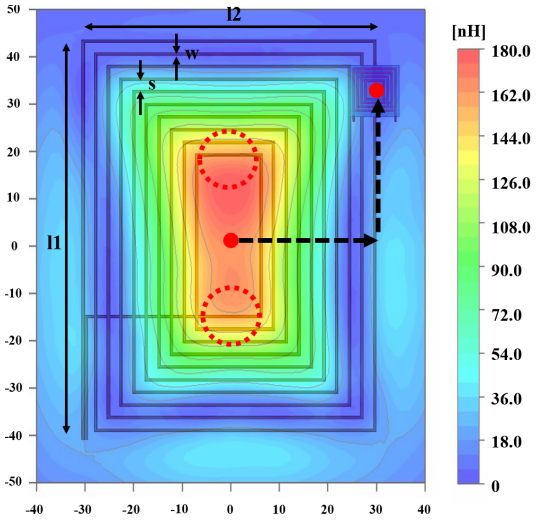

Fig. 7 Mutual inductance between the resonant coil and the ferrite-embedded LTCC.

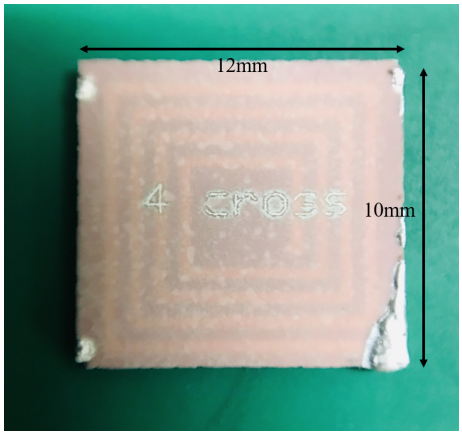

Fig. 8 Fabricated ferrite-embedded LTCC.

to the position is quantitatively expressed. The maximal mutual inductance is 175.8 nH near the center of the transmitting resonant coil. The differences in values were analyzed by applying to the equivalent circuit.

4. WPT System Simulation and Measurement Results

Figure 8 shows a ferrite-embedded LTCC receiver coil fabricated based on the 3D simulation results. Figure 9 shows the board on which the ferrite-embedded LTCC for measurement is mounted. Figure 10 shows the characteristics of the ferrite-embedded LTCC based on simulation results. These quantities were measured at 5–8 MHz around the center frequency. The complicated and difficult manufacturing process contributed to the difference across the samples.

Table 4 summarizes the simulation and measurement results at the frequencies of 1 kHz and 6.78 MHz.

Figure 11 shows the experiment settings. The gap between the transmitting loop coil and the resonant coil, which constitutes the transmitter, is 1.0 mm. The ferrite-embedded

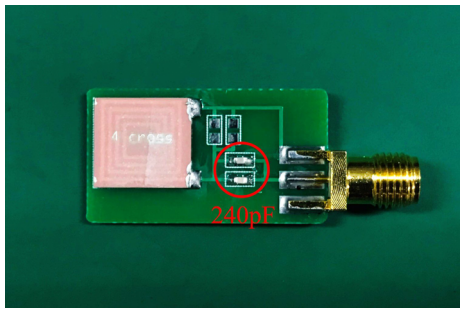

Fig. 9 Ferrite-embedded LTCC receiver coil on the test board.

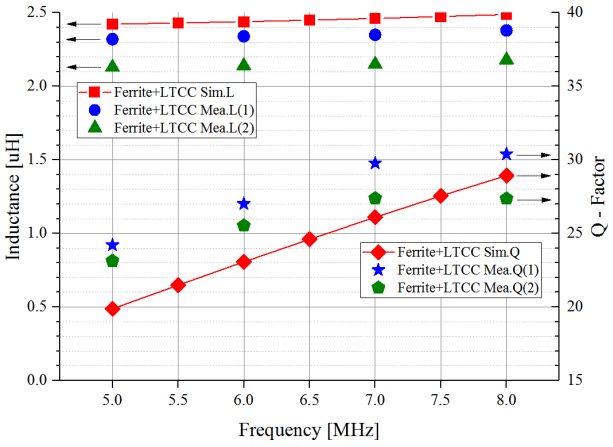

Fig. 10 Simulation and measurement results of the ferrite-embedded LTCC.

Table 4 Simulation and measurement result of the ferrite-embedded LTCC.

	Simulation		Measurement	
Frequency [MHz]	0.001	6.78	0.001	6.78
Inductance [μH]	2.18	2.45	2.36	2.47
Resistance [Ω]	1.06	4.09	1.8	4.2
Q factor	-	25	-	25

LTCC receiver is located where the mutual inductance between the transmitter and the receiver is the greatest in Fig. 7. The ferrite-embedded LTCC receiver and transmitter have distance of 5.0 mm. The transmission characteristics were simulated, measured, and compared. The transmitting resonant coil is connected in series with a 95 pF capacitor, and the ferrite-embedded LTCC is connected in series with a 240 pF capacitor and load. S_{21} and S_{31} are measured simultaneously by using 4 port network analyzer.

Figure 12 shows the experimental setup that applies one receiving ferrite-embedded LTCC. Figure 13 shows the simulation results of the setup in Fig. 12 on frequency sweep. The simulation results and measured S_{21} are -6.7 dB and -7.1 dB, respectively, which results in the power transmission efficiency of approximately 20%.

Figure 14 shows the experimental setup that applies two receiving ferrite-embedded LTCCs. Figure 15 shows the results of the simulation with the setup in Fig. 14 on frequency sweep. The measured S_{21} and S_{31} are -7.9 dB and

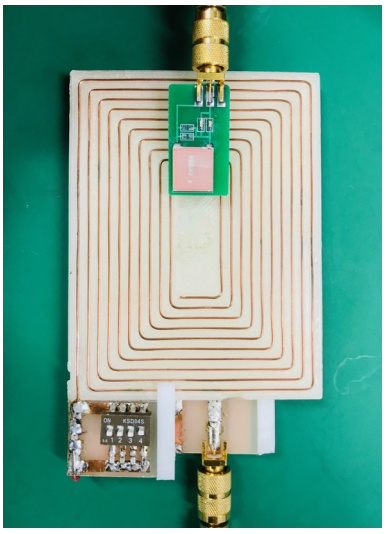

Fig. 11 Setting to measure the proposed system.

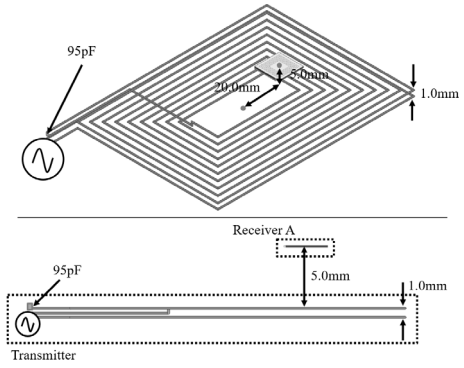

Fig. 12 One receiver with ferrite-embedded LTCC on the WPT transmitter.

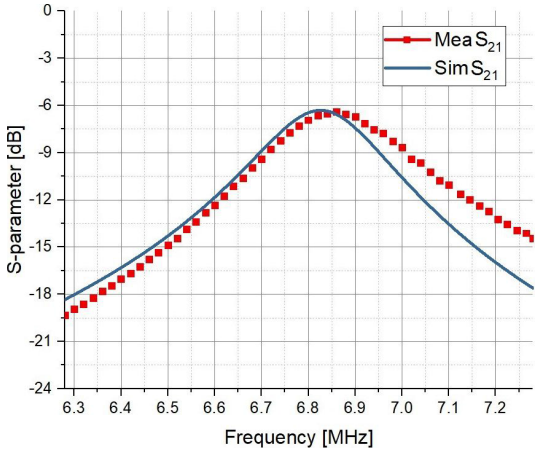

Fig. 13 Simulated and measured $|S_{21}|$ results of one receiver with the ferrite-embedded LTCC for the Fig. 12 configuration.

−7.8 dB, respectively, which results in the summed power transmission efficiency of approximately 32%.

Table 5 shows the efficiency comparison of the target resonant frequency and the frequency from which the maximum efficiency was achieved when two receive LTCCs were applied. These results suggest that a fine adjustment of the resonant frequency is necessary.

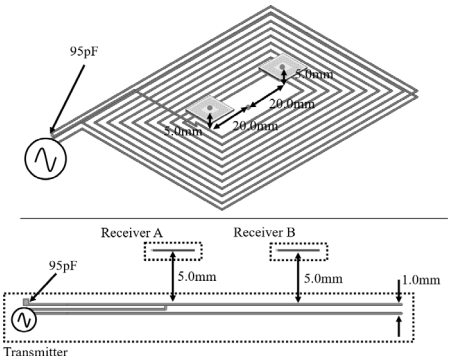

Fig. 14 Two receivers with ferrite-embedded LTCC on the WPT transmitter.

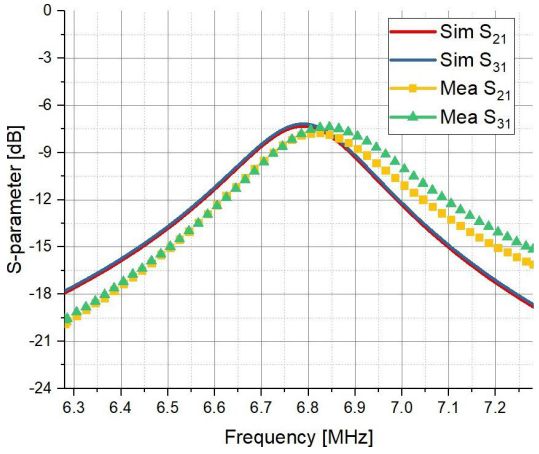

Fig. 15 Simulated and measured $|S_{21}|$ and $|S_{31}|$ results of two receivers with the ferrite-embedded LTCC for the Fig. 14 configuration.

Table 5 Simulation and measurement results of the WPT system ferrite-embedded LTCC for the receivers.

	Receiver A $\lvert S_{21}\rvert$ [dB]	Receiver B $\lvert S_{31}\rvert$ [dB]	Efficiency A, B [%]
Simulation (@6.78 MHz)	−7.3	−7.1	18, 19
Measurement (@6.78 MHz)	−7.9	−7.8	16, 16
Measurement (@6.83 MHz)	−7.7	−7.4	17, 18

5. Conclusion

In this study, a WPT system was constructed in compliance with the 6.78MHz AFA (previous A4WP) specification, which is a global standard for magnetic resonance WPT systems. The proposed magnetic resonance WPT was designed for the SIMO-based multiple-output system with small size receiving coil. To minimize receiving coil dimensions, a receiver with the size of $10.0\times12.0\,\mathrm{mm}^2$ was manufactured by using the ferrite-embedded LTCC technique. The total trans-

mission power efficiency delivered from a $60.0 \times 80.0\,\mathrm{mm}^2$ transmitter to the two receivers was measured by 32%.

The inductance deviation from the manufacturing precision in the LTCC with embedded ferrite may cause failure in the entire module. In addition, the actual application of such ferrite-embedded LTCC may be difficult because of the different firing temperature and low strength due to mixed materials of the ceramic and the ferrite, and the limitation of the inductance value depending on the manufactured size.

This study can contribute to the development of an implantable module through miniaturization, and of the ubiquitous charge via multiple receivers.

References

[1] E. Bou, R. Sedwick, and E. Alarcon, "Scalability analysis of SIMO non-radiative resonant wireless power transfer systems based on circuit models," 2015 IEEE International Symposium on Circuits and Systems (ISCAS), pp.694–697, Lisbon, 2015.
[2] Y.J. Kim, D. Ha, W.J. Chappell, and P.P. Irazoqui, "Selective wireless power transfer for smart power distribution in a miniature-sized multiple-receiver system," IEEE Trans. Ind. Electron., vol.63, no.3, pp.1853–1862, 2016.
[3] A. Uchida, S. Shimokawa, and H. Oshima, "Effect of load dependence of efficiency in a multi-receiver WPT system," 2017 IEEE Wireless Power Transfer Conference (WPTC), pp.1–4, Taipei, 2017.
[4] S.Q. Lee, W.S. Youm, and G. Hwang, "Wireless power transfer technology for implantable medical device," Electronics and Telecommunications Trends, vol.28, no.5, pp.72–82, 2013.
[5] S. Peng, M. Liu, Z. Tang, and C. Ma, "Optimal design of megahertz wireless power transfer systems for biomedical implants," 2017 IEEE 26th International Symposium on Industrial Electronics (ISIE), pp.805–810, Edinburgh, 2017.
[6] L. Li, H. Liu, H. Zhang, and W. Xue, "Efficient wireless power transfer system integrating with metasurface for biological applications," IEEE Trans. Ind. Electron., vol.65, no.4, pp.3230–3239, April 2018.
[7] E.S. Gámez Rodríguez, A.K. RamRakhyani, D. Schurig, and G. Lazzi, "Compact low-frequency metamaterial design for wireless power transfer efficiency enhancement," IEEE Trans. Microw. Theory Techn., vol.64, no.5, pp.1644–1654, May 2016.
[8] Y. Cho, J.J. Kim, D.-H. Kim, S. Lee, H. Kim, C. Song, S. Kong, H. Kim, C. Seo, S. Ahn, and J. Kim, "Thin PCB-type metamaterials for improved efficiency and reduced EMF leakage in wireless power transfer systems," IEEE Trans. Microw. Theory Techn., vol.64, no.2, pp.353–364, Feb. 2016.
[9] A.B. Islam, S.K. Islam, and F.S. Tulip, "Design and optimization of printed circuit board inductors for wireless power transfer system," Circuits and Systems, vol.4, no.2, pp.237–244, 2013.
[10] M. Zargham and P.G. Gulak, "Fully integrated on-chip coil in 0.13 μm CMOS for wireless power transfer through biological media," IEEE Trans. Biomed. Circuits Syst., vol.9, no.2, pp.259–271, 2015.
[11] M. Kováč, V. Stopjaková, D. Arbet, L. Nagy, and J. Brenkuš, "Investigation of on-chip coil in 130 nm standard CMOS for WPT and bio-applications," 2016 International Conference on Emerging eLearning Technologies and Applications (ICETA), pp.177–182, Vysoke Tatry, 2016.
[12] J. Lu, L. Zhang, M. Arakawa, and T. Harada, "Wireless power supply for all-in-one LTCC packaged sensor nodes applicable to infrastructure monitoring" IEEJ Trans. SM, vol.137, no.9, pp.267–271, 2017.
[13] W. Zhong and S.Y.R. Hui, "Auxiliary circuits for power flow control in multifrequency wireless power transfer systems with multiple receivers," IEEE Trans. Power Electron., vol.30, no.10, pp.5902–5910, Oct. 2015.
[14] E. Bou-Balust, A.P. Hu, and E. Alarcon, "Scalability analysis of SIMO non-radiative resonant wireless power transfer systems based on circuit models," IEEE Trans. Circuits Syst. I, Reg. Papers, vol.62, no.10, pp.2574–2583, Oct. 2015.
[15] C. Xu, Y. Zhuang, H. Han, C. Song, Y. Huang, and J. Zhou, "Multi-coil high efficiency wireless power transfer system against misalignment," 2018 IEEE MTT-S International Wireless Symposium (IWS), pp.1–3, Chengdu, 2018.

Young-Hyun Kim received the B.S., M.S. and Ph.D. degrees in Electronics Engineering from Incheon National University, Korea in 1994, 1996, and 2018, respecttively. His research interests include the mobile communication system, design & analysis of microwave circuit, system and wireless power transfer system.

Dae-Kil Park received the B.S. and M.S. degree in Electronics Engineering from Incheon National University in 2014 and 2016, respectively. He is currently in the Ph.D. program in electronics engin-eering, Incheon National University. His research interests include the satellite communication system, design & analysis of microwave circuit, system and wireless power transfer system.

Kyung-Heon Koo received the B.S., M.S. and Ph.D. degrees in Electrical Engineering from Seoul National University, Korea in 1981, 1983, and 1991, respecttively. Since 1983, he has been involved in the design and development of microwave circuits and systems at the Now Precision Co., Seband Precision Co., KT Eng. Co., HaiTaiai Electronics Co, He spent sabbatical leave at the University of California, San Diego, U.S.A., from August 1999 to July 2000. He is currently a professor in the Department of Electronics Engineering, Incheon National University, Korea. His research interests include the design of microwave circuits, multiple mode modules, RADAR and surveillance system.